Surface photovoltage spectroscopy for defect investigation of diamond

N. Schüler1, S. Fengler1, T. Dittrich2, V. Nikonova1, D. Abou-Ras3, Sebastian Weitz3, K. Dornich1

1 Freiberg Instruments GmbH, Delfter Str. 6, 09599 Freiberg, Germany

2 Helmholtz-Zentrum Berlin für Materialien und Energie GmbH, Schwarzschildstr. 8, 12489 Berlin, Germany

3 Helmholtz-Zentrum Berlin für Materialien und Energie GmbH,Hahn-Meitner-Platz 1, 14109 Berlin, Germany

Keywords

diamond, surface photovoltage spectroscopy, modulation, transients, grain boundaries, defects, charge transfer

Abstract

Defect related transition energies and charge transfer along grain boundaries were studied in polycrystalline diamond by using a new type of mirrorless double-prism monochromator based on fused silica and by introducing modulated transient surface photovoltage spectroscopy. Polycrystalline diamond served as a model system containing small crystallites at the seed and large crystallites at the growth sides. Illumination was performed between 0.4 and 7.3 eV for seed and growth side orientations of the sample which allowed for homogeneous excitation of defect related transitions across the sample and for variation of the penetration depth under fundamental absorption in diamond. Photogenerated electrons were separated towards the seed side independently of the defect related transition for excitation below the range of the bandgap of diamond. Under strong absorption, photogenerated electrons were preferentially separated towards the surface. We found that photogenerated electrons are transferred faster than photogenerated holes along grain boundaries and that photogenerated holes are preferentially trapped at defects in crystallites. The enhancement of electron transfer via grain boundaries also explains the observed preferential electron trapping at surface states of diamond.

1. Introduction

Diamond has a huge application potential, for example, in electron emission devices, high power electronics, sensors and electro- and photo-electrochemistry (see, for example the review [1]). Defects and charge transfer processes play a crucial role also in diamond related devices. The density of defects is high at/near grain boundaries, which are major structural defects in diamond grown by chemical vapor deposition (CVD) [2]. Due to the high defect density, hopping transport occurs along grain boundaries [3] and electron emission is enhanced at grain boundaries surrounded by diamond crystallites [4]. It seems well established that sp^2 hybridization plays a crucial role for the formation of defects along grain boundaries in diamond [5] [6] and that defects such as vacancies can segregate at (111) twist grain boundaries in diamond as shown by simulations [7]. However, little is known about the transfer of electrons and/or holes towards defects along grain boundaries and surfaces of diamond.

A surface photovoltage (SPV) arises when photogenerated charge carriers are separated in space [8]. The SPV is defined as the negative light induced change of the contact potential difference between a sample and a measurement electrode. SPV signals can have a positive or negative sign depending on whether positive or negative charge is separated in the direction towards the measurement electrode. Therefore, SPV measurements can provide information about differences in the transfer of photogenerated electrons or holes. For related SPV measurements on diamond samples, a time dependent selectivity of positive and negative SPV components and a highly stable light source tunable continuously from the near infrared to the deep ultraviolet, are required. In this work, modulated transient SPV spectroscopy is introduced for getting rid of slow processes and drift phenomena as in dc measurements, first, and for opening a time window in the ms range for highly sensitive measurements with a very stable light source tunable continuously from the near infrared to the deep ultraviolet, second. A new well suitable light source based a mirrorless double-prism monochromator has been recently presented [9].

A diamond single crystal and a polycrystalline diamond sample with a seed and a growth side have been chosen as model systems for the analysis of defect related transitions and mechanisms of directed charge separation. In polycrystalline diamond, the density of grain boundaries at the seed is much higher than the density of grain boundaries at the growth side (see also the idealized cross section in figure 1 (a)), i.e. phenomena related to charge transfer along grain boundaries will be enhanced towards the seed side. In addition, such a sample exhibits a very broad distribution of defect related transitions in SPV spectra [10] enabling homogeneous excitation across the sample. Transitions include defect-defect related transitions and transitions between defect states and states in the valence or conduction band (see also the idealized band

diagram in figure 1 (b)). Therefore, depending on the transition, electron or hole transfer can occur via defect or extended states in the valence or conduction bands. With the use of the light source tunable over a wide range, the absorption depth in diamond can be varied so that fundamental absorption takes place in different regions of the crystallites. For example, the absorption coefficient of diamond is about 10^3 cm^{-1} and $6 \cdot 10^3$ cm^{-1} at 5.6 and 6.3 eV, respectively [11] corresponding to absorption lengths of 10 and 1.7 µm, respectively.

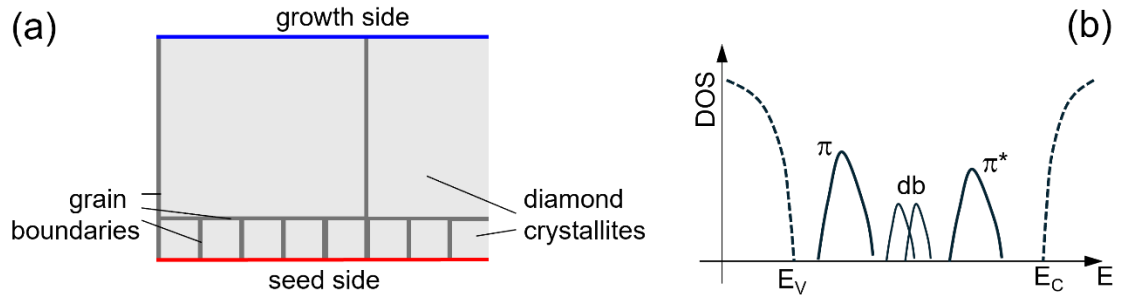

Figure 1: Idealized cross section of CVD diamond with small diamond crystallites near the seed side and large diamond crystallites near the growth side (a) and idealized distribution of the density of states (b).

In this work, it will be shown that the use of the new mirrorless double-prism monochromator based on fused silica together with modulated transient SPV spectroscopy and bias illumination enhances the sensitivity to defect related transitions in diamond single crystals and enables measurements giving information about preferential charge transfer processes in polycrystalline diamond.

2. Experimental

Figure 2 shows a schematic of the experimental set-up used in the experiments. Illumination was performed with a laser driven light source (LDLS, EQ99-X, Hamamatsu). The LDLS was mounted on a specially designed illumination unit containing two adjustable fused silica lenses for collimating and focusing the light (Freiberg Instruments) into the mirrorless double-prism monochromator based on fused silica (DPM100, Freiberg Instruments [9]). The light was directed from the monochromator to the electrode with a specially designed outcoupling unit containing two adjustable fused silica lenses and one fused silica prism and an optical chopper for ac (modulated) SPV measurements (Freiberg Instruments).

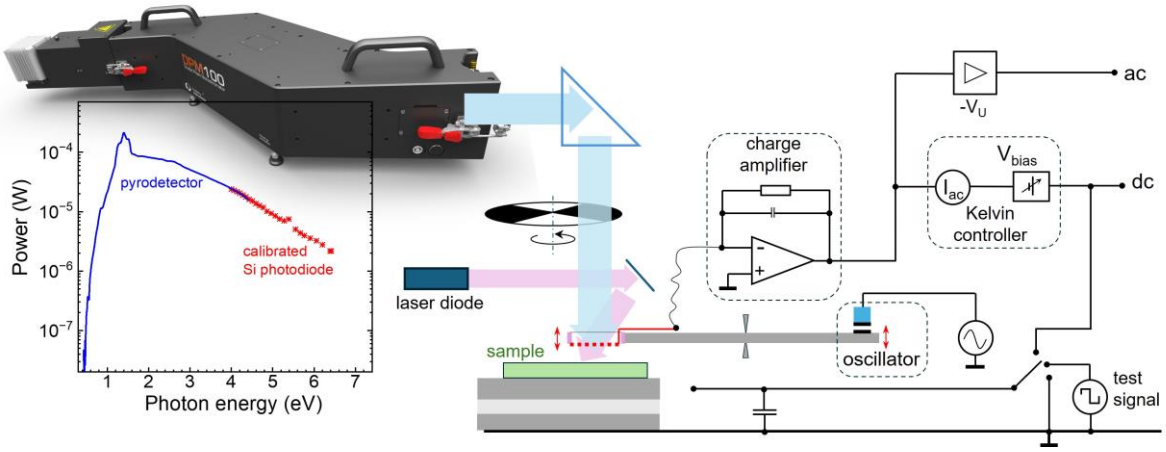

Figure 2: Schematic of the experimental set-up for continuous dc (Kelvin probe regime) and ac (modulated) SPV measurements over very wide spectral range. The set-up includes a laser driven light source, a mirrorless double-prism monochromator based on fused silica (DPM100), a chopper, a laser diode and a mirror for bias illumination, a steel bar with the perforated electrode (vibrating in dc SPV measurement regime, fixed in the ac SPV measurement regime), an isolated sample holder which can be connected with the dc SPV circuit, ground or test signal generator for calibration of ac SPV signals, a charge amplifier and a Kelvin controller. The insert shows the power spectrum of the monochromatic illumination source between 0.4 and 6.4 eV.

The SPV measurements were performed in ambient air. The insert of figure 2 shows the power spectrum of the monochromatic illumination source between 0.4 and 6.4 eV. Above 0.6 eV, the power was higher than 0.1 µW. The maximum power was reached at 1.4 eV (200 µW) and the power decreased to 2 µW at 6 eV. Above 6.5 eV, absorption by oxygen set on (Schuman-Runge bands [12]).

The perforated electrode (diameter 7 mm, Au coated) had the form of a pot and was pressed with a Teflon ring into a grounded steel bar. The steel bar was fixed in the center with two knife edges. For dc (Kelvin probe regime) SPV measurements, a vibration of the steel bar was excited with an oscillator located at the end opposite to the electrode (vibration frequency 1.05 kHz). A charge amplifier (Elektronik Manufaktur Mahlsdorf) was placed close to the electrode for coupling out signals. A Kelvin controller and a test signal generator (Elektronik Manufaktur Mahlsdorf) were used for dc SPV measurements and for calibrating ac SPV signals, respectively. SPV signals were measured with an analog digital converter whereas modulated transient SPV signals were converted to in-phase (X) and phase-shifted by 90° (Y) signals by software.

For demonstrating the potential of ac (modulated) SPV spectroscopy, measurements were performed on single crystalline diamond (Element6, CVD, <110>) and polycrystalline diamond (Diamond Materials) whereas the surfaces of the samples were not modified by additional

treatments. Laser diodes were used for bias illumination at 650, 532 and 405 nm (correspond to photon energies of about 1.9, 2.3 and 3.1 eV which will be referred in the following). It shall be mentioned that diamonds are un-doped so that the Fermi energy is in/near the middle of the bandgap. Defect states below or above the Fermi energy are occupied or unoccupied. For this reason, we chose photon energies of bias light below the half of the bandgap (1.9 eV), around the half of the bandgap (2.3 eV) and above the half of the bandgap (3.1 eV) of diamond in order to excite transitions from occupied to unoccupied defect states, from/into occupied/unoccupied defect states also to extended states and from/into occupied/unoccupied defect states preferentially to extended states, respectively. The intensities of the laser diodes were 3.6, 0.55 and 33 mW for 650, 532 and 405 nm. The sizes of the crystallites were of the order of 1 µm at the seed side and tens of µm at the growth side (Figure 3 (a)). Measurements were performed on the polycrystalline diamond under seed and front side orientations (Figure 3 (b)).

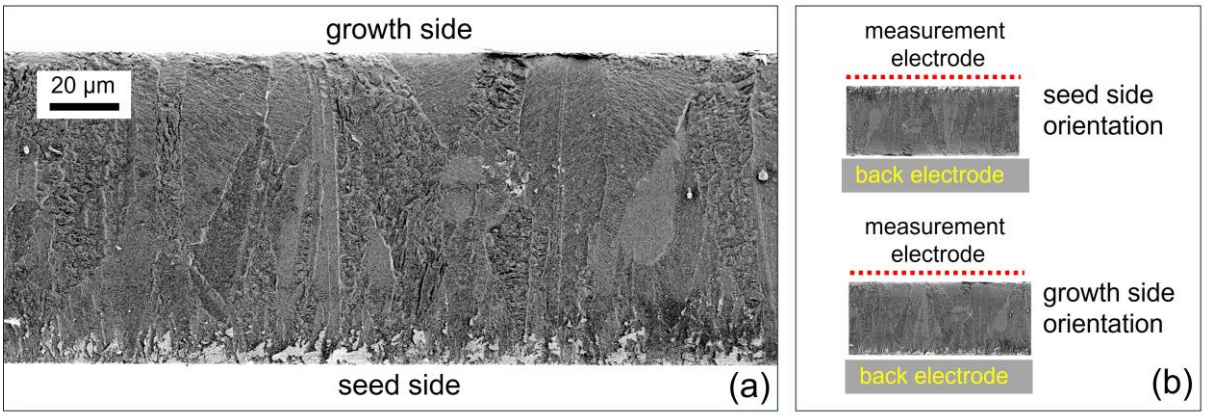

Figure 3: Cross section (un-smoothed) of the polycrystalline diamond made by secondary electron microscopy (a) and schematics for seed and growth side orientations (b). The seed and growth sides are marked in (a).

A characteristic microstructure overview, analyzed by electron backscatter diffraction (EBSD), is given in Figure 4 as a EBSD pattern-quality map (a) and an orientation-distribution map (b). Before performing the EBSD measurements (Zeiss Ultra Plus scanning electron microscope and Oxford Instruments EBSD system), the cross section was smoothed by means of a focused Ar-ion beam (Baltec RES101) at 5 kV and 3.5 mA for 12 h. Twin boundaries were well distinguished from randomly oriented grain boundaries. The fraction of twin boundaries with respect to the complete grain boundary density was about 40%.

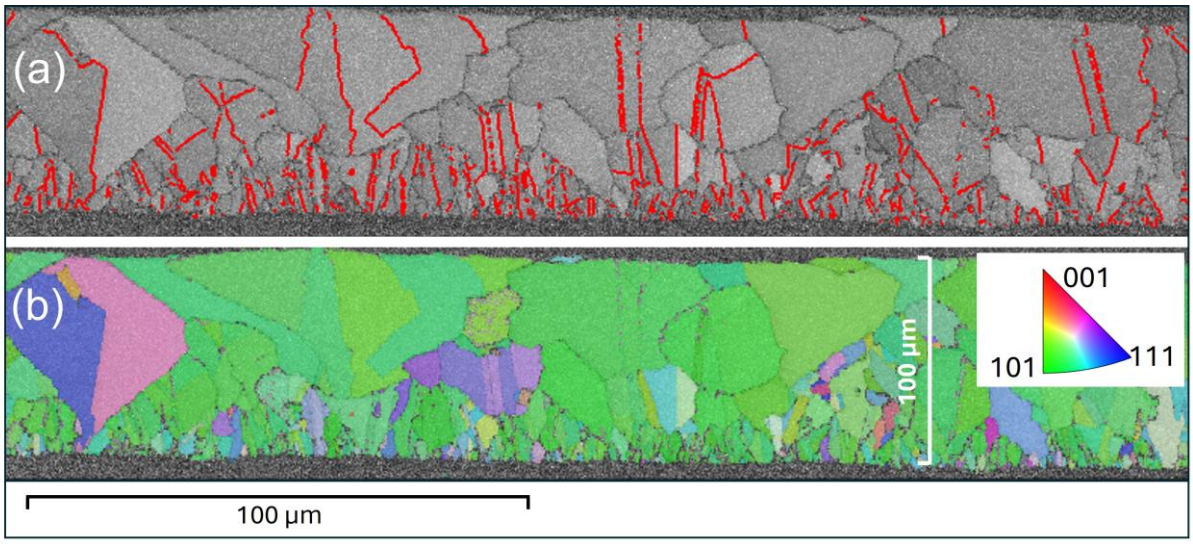

Figure 4: (a) EBSD pattern-quality map with twin boundaries highlighted by red lines and (b) orientation distribution map (same dataset as in a) with the local orientation given as false colors (see legend). The fraction of the twins with respect to the complete grain boundary density is about 40%.

For measuring the modulated SPV spectra, the light was chopped at 8 Hz whereas the chopper was placed close to the exit slit of the monochromator within the outcoupling unit. The corresponding switching between the half periods of light on and light off lasted for 3...4 ms due to the finite spot size of the light beam. The time dependent SPV signals were continuously red out with an ADC (25 kS/s). Incidentally, the modulation frequency of 8 Hz has been chosen as compromise with respect to previous transient measurements that showed slow relaxation of SPV signals [10] to time consumption for measurements.

Contour plots give a map of the time dependent SPV signals as a function of photon energy. The contour plots are given in false colors for logarithmic positive and (inverted) negative) SPV signals whereas the SPV signals were discriminated between -20 and +20 µV.

In-phase (X) and phase-shifted by 90° (Y) SPV signals were obtained by multiplying the time (t) dependent data with sin(t) or cos(t), respectively, and integrating the resulting functions over N = 40 periods (T- period length, see equations (1) and (2)):

$$X = \frac{1}{N \cdot T} \cdot \int_0^{N \cdot T} SPV(t) \cdot \sin(t) \cdot dt \quad (1)$$

$$Y = \frac{1}{N \cdot T} \cdot \int_0^{N \cdot T} SPV(t) \cdot \cos(t) \cdot dt \quad (2)$$

Incidentally, X and Y signals correspond to fast and slow responses in relation to T (see also [13]). The PV amplitude is defined as the square root of the sum of the squared X and Y signals. The arctan of the phase angle is defined by the negative ratio between the Y and X signals.

3. Results and discussion

3.1. Bias illumination for enhanced defect detection in a diamond single crystal

Figures 5 (a) and (b) show the contour plots of the modulated transient SPV spectroscopy for the diamond crystal measured without bias light and under bias illumination at 1.9 eV. Onsets around 5.27 (E_g-E_x-$h\nu_{LO/LA}$, [14]) and 5.53 (E_g-E_x+$h\nu_{TA}$, [14]) eV are clearly distinguished. For the measurement without bias light, SPV signals were around the noise level, and the signals reached a negative maximum of about -3 mV (around 6 eV). Under bias illumination, negative defect related signals appeared, set on around 2.5 eV and the maximum SPV signals increased to more than 10 V. The time dependent SPV signals increased continuously during the half modulation period of light on and decreased continuously during the half modulation period of light off.

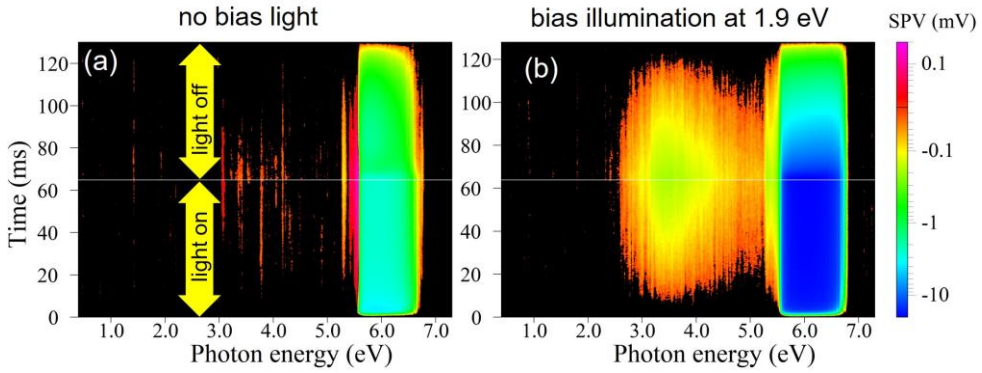

Figure 5: Contour plots of the modulated transient SPV spectroscopy for the diamond single crystal measured without bias light (a) and with bias illumination at 1.9 eV (b). The half modulation periods of light on and light off marked in (a) are identical for all measurements.

The noise can be further reduced in the SPV spectra by the analysis of X and Y signals and the amplitude. Figure 6 shows the spectra of the PV amplitude for the diamond single crystal measured without bias light and measured under bias illumination at 1.9, 2.3 and 3.2 eV. Under bias illumination, defect related signals increased by up to one order of magnitude above the noise level for all photon energies. In comparison to the measurement without bias light, the SPV signals measured above 5.6 eV, i.e. at strong fundamental absorption in diamond, increased by about 9, 7 and 5 times under bias illumination at 1.9, 2.3 and 3.1 eV, respectively.

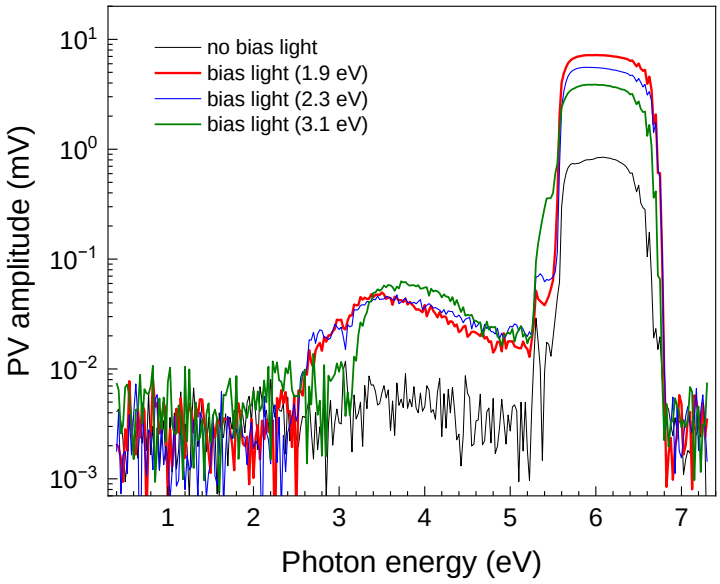

Figure 6: Spectra of the PV amplitude for the diamond single crystal measured without bias light (black line) and under bias illumination at 1.9, 2.3 and 3.1 eV (red, blue and green lines, respectively).

For getting more precise information about onset energies of defect related transitions, it is useful to look closer to the X and Y signals measured below 5.1 eV (figure 7). X signals were of the noise level for measurements without bias light and under bias illumination at 1.9 and 2.3 eV whereas spectral dependent changes were detected in the Y signals, i.e. charge separation and relaxation was much slower than the modulation period. In contrast, spectral dependent changes were detected also in the X signals for the measurement under bias illumination at 3.1 eV. This means that bias illumination at 3.1 eV led to an increase of the conductivity in the diamond crystal due to excitation of mobile charge carriers from defect states closer to the middle of the gap of diamond into extended states in the valence or conduction bands. It can be further concluded that the Fermi energy was around the middle of the bandgap of the diamond crystal since measurements under bias illumination at 2.3 eV did not lead to the appearance of defect related X signals.

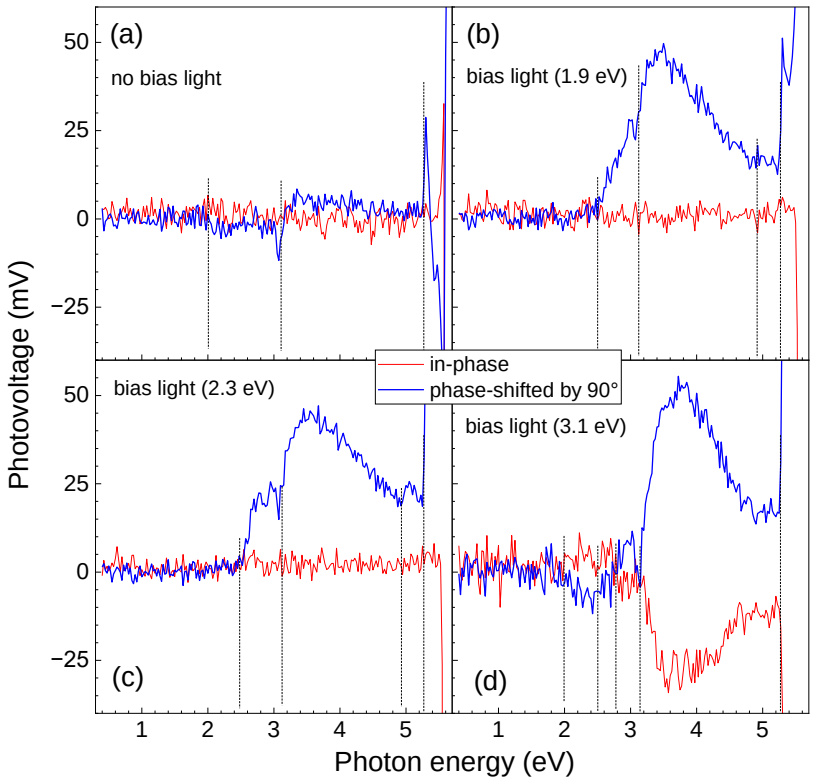

Figure 7: Spectra of the in-phase (red lines) and phase-shifted by 90° (blue lines) signals of the diamond single crystal without bias light (a) and under bias illumination at 1.9, 2.3 and 3.1 eV ((b) – (d), respectively). The vertical dashed lines mark characteristic transition energies.

For the measurement without bias light, the Y signals showed small features setting on around 2 (appearance of negative signals slightly above the noise level) and 3.1 eV (change to positive signals slightly above the noise level). For the measurement under bias illumination at 1.9 and 2.3 eV, positive Y signals set on around 2.5 eV and the slope increased at about 3.1 eV. The decrease in the positive Y signals setting on at about 3.45 (bias illumination at 1.9 eV) or 3.55 eV (bias illumination at 2.3 eV) was caused by the decrease in light intensity. Furthermore, a little feature related to a defect transition appeared at 4.9 eV.

The noise was larger for the measurement under bias illumination at 3.1 eV in comparison to the other measurements, i.e. potential fluctuations across the diamond increased. Transition energies were detected around 2 (onset of positive X and negative Y signals), 2.5 (change of Y signals towards positive signals), 2.8 (change of X signals towards negative signals) and 3.1 eV (onset of a further change of X signals towards more negative signals and increase of the slope of Y signals) eV. Incidentally, the assignment of related transition energies to certain defects is out of the scope of this work.

3.2. Bias illumination for enhanced defect detection in a diamond single crystal

Figure 8 shows the characteristic -ΔCPD spectra of the polycrystalline diamond under seed and growth side orientations. Changes of the slope towards more positive (or less negative) values are related to positive SPV signals and correspond to the onset of transitions leading to a decrease of positive charge in the direction to the measurement electrode. Vice versa, changes of the slope towards more negative (or less positive) values are related to negative SPV signals and correspond to the onset of transitions leading to an increase of negative charge in the direction to the measurement electrode. For growth side orientation, positive and negative SPV signals set on at about 1 and 1.65 eV and at 1.22 eV, respectively, for major defect related transitions. For seed side orientation, the SPV signals were inverted for the defect related transitions. In the range of transitions around the bandgap of diamond, positive SPV signals set on at 5.27 (E_g-E_x-$h\nu_{LO/LA}$, [14]) and 5.48 (E_g-E_x+$h\nu_{TA}$, [14]) eV and negative SPV signals appeared above 5.6 eV (E_g+$h\nu_{LO/LA}$, [14]) for growth side orientation. For seed side orientation, positive SPV signals set also on at 5.27 eV and the evolution of negative SPV signals started above 5.32 eV (E_g-E_x-$h\nu_{TA}$, [14]) and increased strongly at 5.5 eV, what could not be related to a given transition and shall be caused therefore by a qualitative change due to a change in the absorption depth. Therefore, the SPV signals were negative for both growth and seed side orientations for strong absorption starting in the bandgap region. However, these findings do not allow to draw conclusions regarding specific charge transfer processes.

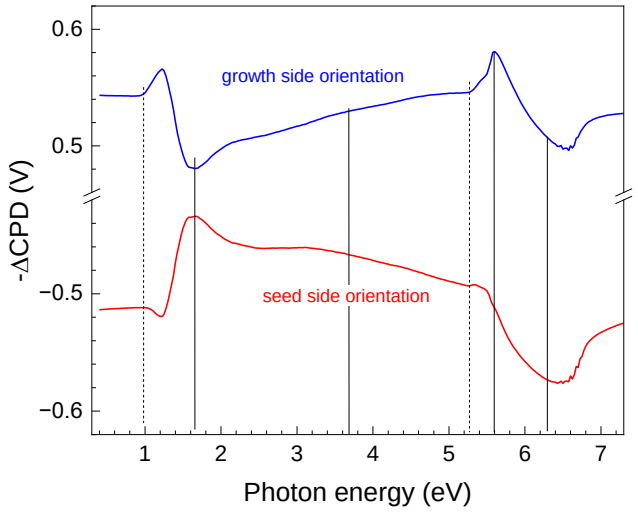

Figure 8: Characteristic spectra of -ΔCPD signals for seed (red) and growth (blue) side orientations. The dashed lines show characteristic onsets of signals around 1 eV and 5.27 (E_g-E_x-$h\nu_{LO/LA}$), the solid lines mark some energies for photogeneration for excitation of defect related transitions (1.65 and 3.7 eV) and for excitation by fundamental absorption in diamond (5.6 and 6.3 eV).

Figure 9 shows the contour plots of the modulated transient SPV spectroscopy for seed and growth side orientations of polycrystalline diamond and the extracted in-phase and phase-shifted by 90° SPV signals. The half modulation periods of light on and light off marked in figure 5 (a) lasted for 62.5 ms. The SPV signals set on at about 1 eV for all measurement conditions.

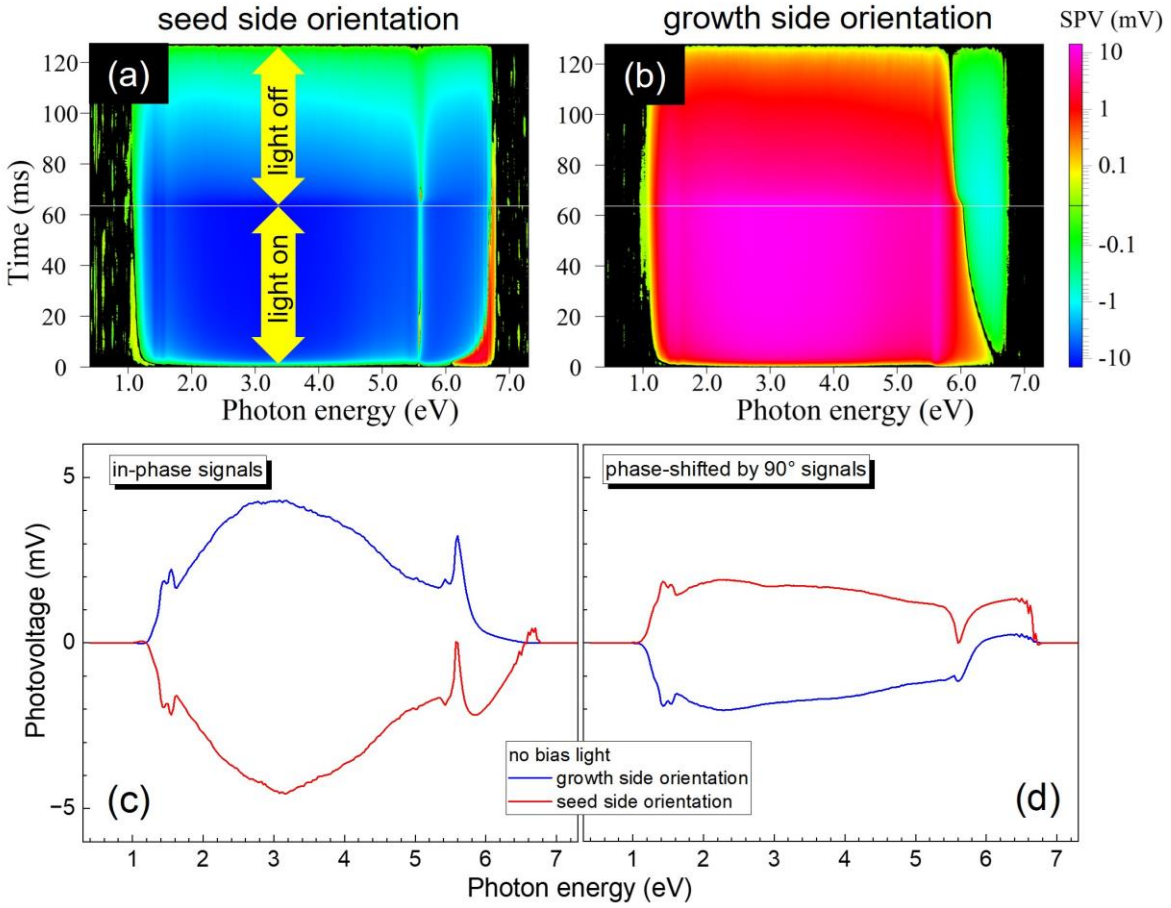

Figure 9: Contour plots of the modulated transient SPV spectroscopy for seed (a) and growth (b) side orientations and extracted spectra of the in-phase (c) and phase-shifted by 90° (d) SPV signals for growth side and seed side orientations (blue and red lines). The half modulation periods of light on and light off marked in (a) are identical for all measurements.

For measurements under seed side orientation, the SPV signals were negative over nearly the whole spectral and time ranges excepting narrow ranges around 1 eV at times up to 40 ms, around 5.6 eV for few time values around 15 and 65 ms and between about 6 and 6.8 eV for time ranges of few ms (at 6 eV) up to about 90 ms (at 6.8 eV). The negative and positive SPV signals reached values up to -10 and +1 mV.

For measurements under growth side orientation, the SPV signals were positive between 1 (over the whole time range) and 5.8 (times longer than 70 ms) to 6.5 (few ms) eV. The SPV signals were

negative between 5.8 (times longer than 70 ms) to 6.5 (few ms) and 6.8 eV. The positive and negative SPV signals reached values up to +10 and -1 mV.

The X and Y signals dominated the broad spectra. Below the range of the band gap, the spectra measured for growth and seed side orientations had a nearly perfect inversion symmetry of the positive and negative signs of the SPV signals. This was not the case for absorption above about 5.4 eV. For getting a deeper understanding of underlying mechanisms of charge separation, a closer look at modulated SPV transients is very helpful. Characteristic time dependent SPV signals extracted at 1.65, 3.7, 5.6 and 6.3 eV (marked also in figure 8) are depicted in figure 10 for measurements under seed and growth side orientations. Incidentally, photon energies of 1.65 and 3.7 eV correspond to excitation of defect related transitions whereas photon energies of 5.6 and 6.3 eV correspond to fundamental absorption in diamond.

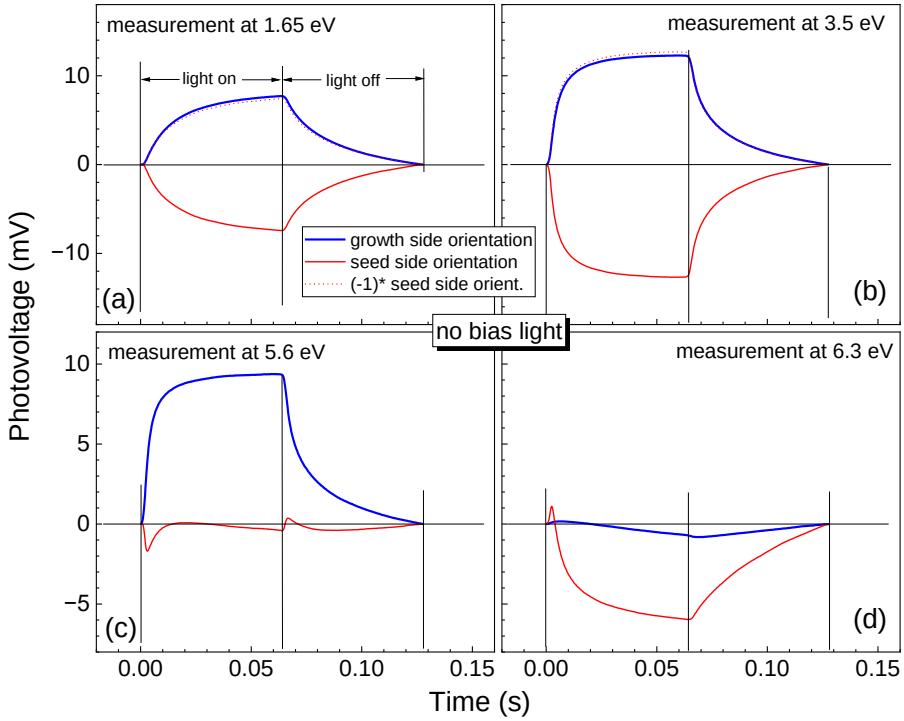

Figure 10: Transients measured for growth (blue lines) and seed (red lines) side orientations at photon energies of 1.65 (a), 3.7 (b), 5.6 (c) and 6.3 (d) eV. The dashed red lines are the transients measured for seed side orientations after inversion.

During the half periods of light on or light off (called light on and light off in the following), the positive and negative SPV signals increased or decreased monotonously for the time dependent SPV signals extracted at 1.65 eV and 3.7 eV nm for growth side orientation whereas the inverted negative time dependent SPV signals of the seed side orientation were practically identical to the positive time dependent SPV signals. Maximum SPV signals of 7.7 mV and 12.4 mV were reached for extraction at 1.65 and 3.7 eV, respectively. The monotonous character and the inversion

symmetry mean that the time dependent SPV signals extracted at 1.65 and 3.7 eV were caused by the same process of modulated charge separation and relaxation for both orientations, i.e. the SPV signals originated from the same region in the sample.

The positive SPV signals extracted at 5.6 eV under growth side orientation increased to a maximum of 9.4 mV and decreased monotonously during light on and light off. In contrast, the positive SPV signals extracted at 6.3 eV increased up to 0.2 mV at 6 ms and decreased and changed to negative values at longer times under growth side orientation. The negative SPV signal reached -0.6 mV at 62.5 mV, increased to -0.8 mV at 67 ms, i.e. during switching to light off, and decreased to 0 mV at 125 ms.

The very different characters of the time dependent SPV signals extracted for growth side orientation at 5.6 and 6.3 eV mean that the penetration depth of the light plays a crucial role for the direction of charge separation. The absorption length in diamond is 10 µm for excitation at 5.6 eV as mentioned before. Therefore, the crystallites at the growth side were illuminated up to internal grain boundaries for excitation at 5.6 eV. On the other hand, the absorption length in diamond is about 1.5 µm for excitation at 6.3 eV in growth side orientation, i.e. light did not reach internal grain boundaries under illumination at 6.3 eV. The time dependent SPV signals were rather similar for extraction at 1.65, 3.7 and 5.6 eV. It can be concluded that the positive SPV signals were caused by charge separation near internal grain boundaries under growth side orientation.

The time dependent SPV signals extracted at 5.6 eV under seed side orientation reached a negative maximum of -1.7 mV at 3 ms, i.e. within the switching from light off to light on. At longer times, the negative SPV signals decreased, changed to positive sign, reached a very small positive maximum of 0.1mV at 20 ms, decreased, changed sign for a second time and reached a value of -0.4 mV at 62.5 ms. During switching from light on to light off, the SPV signals changed sign, reached 0.4 mV at 66 ms, decreased, changed sign again, reached -0.4 mV at 80 ms, and decreased again. The changes of sign gave evidence that three different processes of charge separation participated in the formation of the SPV signals under illumination at 5.6 eV of the seed side.

The time dependent SPV signals extracted at 6.3 eV under seed side orientation reached a positive maximum of 1 mV at 3 ms, i.e. within the switching from light off to light on. At longer times, the positive SPV signals decreased, changed to negative sign and reached a maximum of -6 mV at 65 ms, i.e. within the switching from light on to light off. The negative SPV signals decreased monotonously during light off.

Photogeneration by excitation of defect states or by fundamental absorption near grain boundaries led to positive SPV signals. It has been argued by Nebel et al. that the density of deep hole traps is much higher than the density of deep electron traps in crystallites of polycrystalline

CVD diamond and that for this reason the probability of photogenerated electrons to reach grain boundaries is much higher than for photogenerated holes [15]. At the same time, the drift length is of the order of 1 – 2.6 µm for photogenerated charge carriers in polycrystalline CVD diamond [16] and negative charge is collected near the anode in ion beam induced charge experiments [17], i.e. holes are trapped in the crystallites. Therefore, it can be concluded that charge separation is dominated by the motion of photogenerated electrons in polycrystalline CVD diamond.

Electrons photogenerated at grain boundaries or in crystallites within a distance of 1 – 2.6 µm to grain boundaries move along grain boundaries. The probability for this motion is higher in the direction of increasing density of grain boundaries, i.e. towards the seed side. The enhancement of electron transfer via grain boundaries also explains the higher SPV signals for excitation under seed side orientation than under growth side orientation. The change of the sign of SPV signals under seed side orientation at intermediate depth of fundamental absorption can be explained by a faster electron trapping to grain boundaries with preferential parallel orientation than electron transfer towards the surface via grain boundaries with preferential perpendicular orientation. Furthermore, electron and hole traps are present at the surfaces of diamond. Electrons photogenerated under strong absorption near a diamond surface are preferentially separated towards the surface and cause therefore negative SPV signals.

The dynamics of photogenerated charge carriers depend on illumination with bias light due to excitation of trapped charge carriers. Figure 11 compares modulated SPV transients detected at 1.65 (defect related absorption), 5.6 (absorption length about 10 µm) and 6.3 eV (absorption length about 1 µm) without bias light and under bias illumination at about 1.9, 2.3 and 3.1 eV.

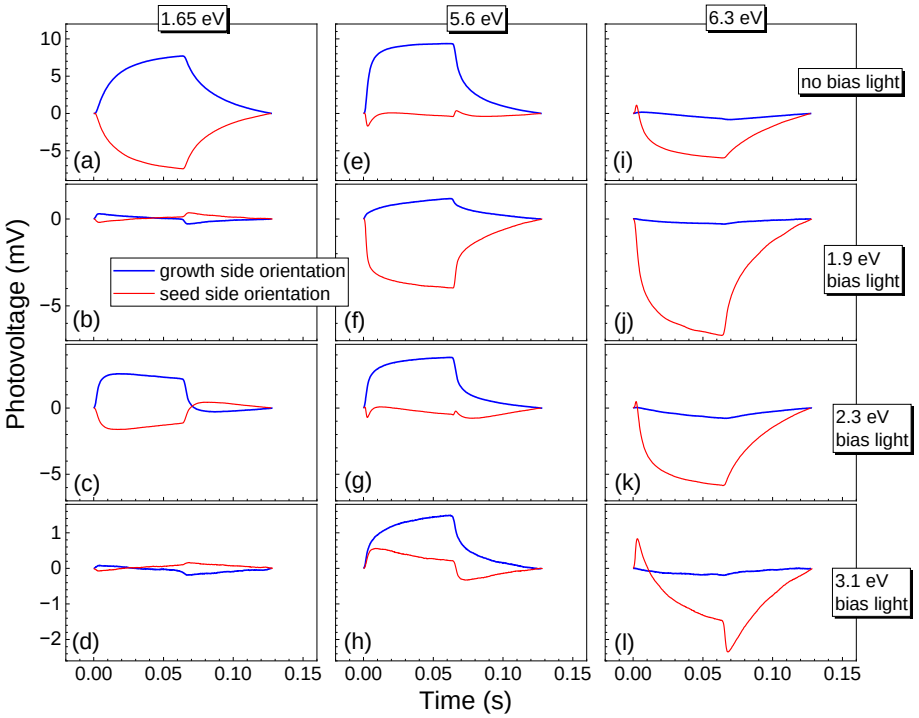

Figure 11: Transients for growth (blue lines) and seed (red lines) side orientations excited at 1.65 (a – d), 5.6 (e – h) and 6.3 (i – l) eV without bias light ((a), (e) and (i)) and under bias illumination at about 1.9 ((b), (f) and (j)), 2.3 ((c), (g) and (k)) and 3.1 ((d), (h) and (l)) eV.

The modulated SPV transients detected at 1.65 eV qualitatively conserved the sign inversion symmetry for seed and growth side orientations under bias illumination. However, there were drastic changes in the dynamic behavior. Under bias illumination at 1.9 and 3.1 eV, the maximum of the positive and negative SPV signals for growth and seed side orientations was reached within the switching from light on to light off and amounted only to 0.3 and -0.2 mV (1.65 eV) and 0.08 and -0.07 mV (3.1 eV), respectively, and the signs changed at 28 and 21 ms (seed side orientation) and 60 and 30 ms (growth side orientation), i.e. during light on. This means that separation of photogenerated holes towards the seed side overwhelmed the separation of photogenerated electrons during light on. Furthermore, the positive (seed side orientation) and negative (growth side orientation) SPV signals reached a maximum of 0.35 and -28 mV (bias light at 1.9 eV) and 0.16 and -0.18 mV (bias light at 3.1 eV) within the switching from light on to light off, i.e. electrons relaxed much faster than holes separated towards the seed sight under bias illumination at 1.9 and 3.1 eV.

For bias illumination of 2.3 eV and detection at 1.65 eV, the maximum of the positive and negative SPV signals was 2.6 (growth side orientation) and -1.6 mV (seed side orientation). After reaching the maximum at 18 ms, the positive and negative SPV signals decreased to 2.2 and -1.1 mV at 64 ms. This means that the separation of photogenerated holes towards the seed side increased during light on but remained by far behind the separation of photogenerated electrons. The SPV

signals decreased rapidly after switching from light on to light off, changed the sign around 70 ms and reached a maximum of 0.43 (seed side orientation) and -0.25 mV (growth side orientation) around 85 ms. The change of the sign during light off shows that the electrons relaxed much faster than holes separated towards the seed sight under bias illumination of 2.3 eV.

The modulated SPV transients measured under growth side orientation and detected at 5.6 did not change qualitatively. The corresponding transients reached a maximum of 9.4 (without bias light) and of 1.2, 3.8 and 1.5 mV under bias illumination of 1.9, 2.3 and 3.1 eV. The decrease of the positive SPV signals under bias illumination can be well explained by enhanced recombination due to de-trapping of holes near internal grain boundaries. The excitation of holes trapped near grain boundaries was most effective for bias illumination at 1.9 eV.

The maximum of the negative SPV signals measured under growth side orientation and detected at 6.3 eV was -0.8 (without bias light) and -0.3, -0.78 and -0.19 mV under bias illumination at 1.9, 2.3 and 3.1 eV, respectively. The comparison with the maximum values detected at 5.6 eV shows that charge separation towards the surface of the growth side was less affected by bias light.

The modulated SPV transients measured under seed side orientation and detected at 5.6 and 6.3 eV changed drastically. A maximum of negative SPV signals of -4 and -6.7 mV was reached under bias illumination at 1.9 eV and for detection at 5.6 and 6.3 eV, respectively, after 63 ms. Furthermore, the local positive maximum at 3 ms disappeared. This means that the corresponding separation of photogenerated electrons and holes towards the surface of the seed side was enhanced and reduced, respectively, under bias illumination at 1.9 eV. Under bias illumination at 2.3 eV, the modulated SPV transients detected at 5.6 and 6.3 eV were qualitatively like those measured without bias light.

Under bias illumination at 3.1 eV, the SPV signals detected at 5.6 eV were positive during light on, increased to 0.56 mV at 8 ms, decreased to 0.22 mV at 64 ms, changed the sign at 66 ms and reached a negative maximum of -0.32 mV at 73 ms. Therefore, bias illumination led to an enhanced separation of photogenerated electrons towards internal grain boundaries so that holes separated towards the surface of the seed side could dominate the SPV signals light on. Under bias illumination at 3.1 eV, the SPV signals detected at 6.3 eV were positive in the beginning, increased to 0.84 mV at 3 ms, changed the sign at 10 ms, reached negative values of -1.5 and -2.4 mV after 64 and 68 ms. The rapid change of the SPV signals from 0.22 to -0.32 mV during the change from light on to light off gives evidence that holes relaxed much faster than electrons separated towards the surface of the seed side. The fact that the SPV signals were much larger for detection at 6.3 eV than for detection at 5.6 eV under bias illumination at 3.1 eV shows that separation of photogenerated electrons towards internal grain boundaries competes with

separation of photogenerated electrons towards the surface of the seed side. This is not surprising since the drift (or transport) length is of the same order as the grain size at the seed side.

4. Conclusions

It has been shown that the new mirrorless double prism monochromator enables continuous surface photovoltage measurements on diamonds from the near infrared to the deep ultraviolet so that defect related transitions can be studied and the range of photogeneration by fundamental absorption can be varied.

The sensitivity to defect related transitions in single crystals of diamond has been drastically increased by applying bias illumination of different photon energies below the bandgap of diamond in modulated transient SPV spectroscopy. Bias illumination from localized into localized states resulted in a strong increase of phase-shifted by 90° SPV signals of defect related transitions, i.e. in very slow modulated SPV responses. In contrast, photogeneration from localized into extended states in a diamond crystal resulted also in a strong increase of the in-phase SPV signals of defect related transitions, i.e. in much faster modulated SPV responses. In future, it will be interesting to vary continuously also the photon energy of bias light.

The modulated time response of SPV signals depended strongly on growth or seed side orientation of the polycrystalline diamond and on the photon energy of the bias light. Without bias illumination, SPV signals were dominated by fast trapping of photogenerated holes in crystallites and preferential electron transfer towards grain boundaries and surfaces. Under bias illumination, de-trapped holes moved also to grain boundaries and surfaces and, depending on the photon energy of bias light, stayed there for longer or shorter time than photogenerated electrons. In future, it will be important to separate surface related from bulk and grain boundary related defect transitions by varying preparation conditions of diamonds and their surfaces. In this context, it will also be important to investigate the specific role of surface roughness.

The method of modulated SPV spectroscopy opens new opportunities for monitoring defect related transitions in diamonds and correlating them with technological treatments and relevant device parameters. For this purpose, it will be also important to gain deeper insight into the specific sense of scale of SPV spectroscopy.

Acknowledgement

The authors are grateful to Florian Ruske (HZB) for taking the SEM image.

References

[1] R. Zulkharnay, P. W. May, Applications of diamond films: a review, Functional Diamond 4 (2024) 2410160, DOI: 10.1080/269411112.2024.2410160.

[2] P. J. Fallon, L. M. Brown, Analysis of chemical-vapour-deposited diamond grain boundaries using transmission electron microscopy and parallel electron energy loss spectroscopy in a scanning transmission electron microscope, Diamond and Related Materials, 2 (1993) 1004, DOI: 10.1016/0925-9635(93)90265-4.

[3] B. Fiegl, R. Kuhnert, M. Ben-Chorin, F. Koch, Evidence for grain boundary hopping transport in polycrystalline diamond films, Appl. Phys. Lett. 65 (1994) 371, DOI: 10.1063/1.112379.

[4] R. Harniman, P. W. May, O. J. L. Fox, Direct observation of electron emission from CVD diamond grain boundaries by tunneling atomic force microscopy independent of surface morphology, Diamond & Related Materials 80 (2017) 147, DOI: 10.1016/j.diamond.2017.09.009.

[5] F, Cleri, P. Keblinski, L. Colombo, D. Wolf, S. R. Phillpot, On the electrical activity of sp^2-bonded grain boundaries in nanocrystalline diamond, Europhys. Lett. 46 (1999) 671, DOI: 10.1209/epl/i1999-00318-5.

[6] P. Steneteg, V. Chirita, N. Dubrovinskaia, L. Dubrovisnky, I. A. Abrikosov, Missing-atom structure of diamond $\Sigma 5$ (001) twist grain boundary, Phys. Rev. B 84 (2011) 144112, DOI: 10.1103/PhysRevB.84.144112.

[7] C. Baruffi, C. Brandl, Vacancy segregation and intrinsic coordination defects at (111) twist grain boundaries in diamond, Acta Materialia 260 (2023) 119253, DOI: 10.1016/j.actamat.2023.119253.

[8] L. Kronik, Y. Shapira, Surface photovoltage phenomena: theory, experiment, and applications, Surf. Sci. Rep. 37 (1999) 1, DOI: 10.1016/S0167-5729(99)00002-3.

[9] T. Dittrich, S. Fengler, M. Franke, Mirrorless fused silica based double-prism monochromator for continuous measurements from the near infrared to deep ultraviolet, Appl. Opt. 63 (2024) 6880, doi: 10.1364/AO.529366.

[10] T. Dittrich, S. Fengler, Transitions in polycrystalline diamond probed by steady state, modulated and transient surface photovoltage spectroscopy, Semicond. Sci. Technol. 38 (2023) 015015, doi: 10.1088/1361-6641/aca788.

[11] H. R. Phillip, E. A. Taft, Kramers-Kronig analysis of reflectance data for diamond, Phys. Rev. 136 (1964) A1445, DOI: 10.1103/PhysRev.136.A1445.

[12] R. E. Huffman, Absorption cross-sections of atmospheric gases for use in astronomy, Canad.J. Chem. 47 (1969) 1823, DOI: 10.1139/v69-298.

[13] T. Dittrich, S. Fengler, Surface photovoltage analysis of photoactive materials, World Scientific (New Jersey, London, Singapore, Beijing, Shanghai, Hong Kong, Taipei, Chennai, Tokyo) (2020).

[14] C. D. Clark, P. J. Dean, V. P. Harris, Intrinsic edge absorption in diamond, Proc. R. Soc. Lond A277 (1964) 312, DOI: 10.1098/rspa.1964.0025.

[15] C. E. Nebel, A. Waltenspile, M. Stutzmann, M. Paul, L. Schäfer, Persistent photocurrents in CVD diamond, Diamond and Related Materials 9 (2000) 404, DOI: 10.1016/S0925-9635(99)00204-6.

[16] C. E. Nebel, M. Stutzmann, F. Lacher, P. Koidl, R. Zachai, Carrier trapping and release in CVD-diamond films, Diamond and Related Materials 7 (1998) 556, DOI: 10.1016/S0925-9635(97)00203-3.

[17] S. M. Hearne, D. N. Jamieson, E. Trajkov, S. Prawer, Temperature-dependent emptying of grain boundary charge traps in chemical vapor deposited diamond, Appl. Phys. Lett. 84 (2004) 4493, DOI: 10.1063/1.1756201.

Graphical abstract